

Off-chip passivated-electrode, insulator-based dielectrophoresis ($O\pi$ DEP)

Phillip Zellner · Tyler Shake · Ali Sahari ·
Bahareh Behkam · Masoud Agah

Received: 4 April 2013 / Revised: 24 May 2013 / Accepted: 5 June 2013 / Published online: 30 June 2013
© The Author(s) 2013. This article is published with open access at Springerlink.com

Abstract In this study, we report the first off-chip passivated-electrode, insulator-based dielectrophoresis microchip ($O\pi$ DEP). This technique combines the sensitivity of electrode-based dielectrophoresis (eDEP) with the high-throughput and inexpensive device characteristics of insulator-based dielectrophoresis (iDEP). The device is composed of a permanent, reusable set of electrodes and a disposable, polymer microfluidic chip with microposts embedded in the microchannel. The device operates by capacitively coupling the electric fields into the microchannel; thus, no physical connections are made between the electrodes and the microfluidic device. During operation, the polydimethylsiloxan (PDMS) microfluidic chip fits onto the electrode substrate as a disposable cartridge. $O\pi$ DEP uses insulating structures within the channel as well as parallel electrodes to create DEP forces by the same working principle that iDEP devices use. The resulting devices create DEP forces which are larger by two orders of magnitude for the same applied voltage when compared to off-chip eDEP designs from literature, which rely on parallel electrodes alone to produce the DEP forces. The larger DEP forces allow the $O\pi$ DEP device to operate at high flow rates exceeding 1 mL/h. In order to demonstrate this technology, *Escherichia coli* (*E. coli*), a known waterborne pathogen, was trapped from water samples. Trapping efficiencies of 100 % were obtained at flow rates as high as 400 μ L/h and 60 % at flow rates as high as 1200 μ L/h. Additionally,

bacteria were selectively concentrated from a suspension of polystyrene beads.

Keywords Dielectrophoresis (DEP) · Microfluidic · Insulator-based dielectrophoresis (iDEP) · *Escherichia coli* (*E. coli*) · Microfabrication

Abbreviations

CE	capture efficiency
DEP	Dielectrophoresis
eDEP	electrode-based dielectrophoresis
GFP	Green Fluorescent Protein
iDEP	insulator-based dielectrophoresis
nDEP	negative DEP
$O\pi$ DEP	Off-chip passivated-electrode, insulator-based dielectrophoresis microchip
pDEP	positive DEP
PDMS	polydimethylsiloxan

Introduction

Dielectrophoresis (DEP) is a well-known electric field based technique for separating, moving, and trapping micron-scale particles. DEP has been shown to be particularly useful for characterizing biological cells. The small size of cells (~1–10 μ m) allow for the necessary high electric fields to be generated with relatively low applied voltages. The other strength of DEP is that it allows for many independent variables, such as signal magnitude, signal frequency, signal waveform, and electrode spacing to be used to control the manipulation. This results in the ability to separate very similar particles. Thus, the technique has spread to a wide range of biological applications, including bacteria [1], yeast [2], mammalian cells [3], viruses [4], and proteins [5].

Traditionally, electrode-based DEP (eDEP) devices create nonuniform fields with electrode designs including sharp

Electronic supplementary material The online version of this article (doi:10.1007/s00216-013-7123-7) contains supplementary material, which is available to authorized users.

P. Zellner · T. Shake · M. Agah (✉)
VT MEMS Lab, Department of Electrical and Computer
Engineering, Virginia Tech, Blacksburg, VA 24060, USA
e-mail: agah@vt.edu

A. Sahari · B. Behkam (✉)
MicroN BASE Lab, Department of Mechanical Engineering,
Virginia Tech, Blacksburg, VA 24060, USA
e-mail: behkam@vt.edu

electrodes and narrowly spaced electrodes [6–9]. Indeed, the majority of DEP devices reported in literature utilize microfabricated electrodes. The use of micropatterned electrodes allows for strong local electric fields; however, it increases the cost and complexity of fabrication. For biological applications, avoiding contamination and device cost are concerns; thus, it is desirable for the microfluidic components to be low-cost and disposable.

Alternatively, insulator-based DEP (iDEP) uses insulating structures rather than electrode arrays to produce the nonuniform fields needed to drive DEP and to remove the threat of gas evolution due to electrolysis [10]. iDEP microfluidic devices have been used to manipulate a wide range of particles including bacteria, viruses, cells, and beads [11–14]. In iDEP devices, the electric voltages are applied along the entire length of the microchannels, which leads to a large heat buildup [15]. Also, the electrodes must be brought in contact with the solution, which can lead to contamination issues.

In this paper, we present the first reported off-chip passivated-electrode, insulator-based dielectrophoresis microchip (OπDEP). This technique allows for inexpensive devices to create strong DEP forces with low Joule heating, leading to a high throughput microfluidic system. Our device uses insulating structures within the channel as well as parallel electrodes to create DEP forces by the same working principle that iDEP devices use. Additionally, unlike eDEP and iDEP, no physical electric connections are made to the microfluidic chip. Thus, a new, inexpensive microfluidic chip may be used for each experiment while the electrodes may be reused. The resulting devices create DEP forces, which are larger by roughly two orders of magnitude for the same applied voltage compared with eDEP, which relies on parallel electrodes alone to produce the DEP forces. In order to demonstrate this technology, we trapped *Escherichia coli* (*E. coli*), a known waterborne pathogen, from water samples at flow rates as high as 1200 μL/h.

We also selectively concentrated bacteria from a suspension of polystyrene beads.

Theory

A schematic of the OπDEP devices is shown in Fig. 1. The device is composed of a permanent, reusable set of electrodes and a disposable, polymer microfluidic chip with microposts embedded in the channel. The microfluidic chip fits onto the electrodes as a disposable cartridge. The device operates by capacitively coupling the electric fields into the microfluidic channel. Figure 1c shows the dominant forces acting on a particle within the device. The main force balance that occurs on a particle is between the dielectrophoresis force and the hydrodynamic drag force.

Dielectrophoresis is the motion of polarizable particles that are suspended in an electrolyte when subjected to a spatially nonuniform electric field [16]. The DEP force felt by a spherical particle suspended in a medium is:

$$F_{DEP} = 2\pi R^3 \epsilon_m \text{Re}[f_{CM}] \nabla(\mathbf{E} \cdot \mathbf{E}) \tag{1}$$

where R is the radius of the particle, ϵ_m is the permittivity of the medium, \mathbf{E} is the local electric field. $\text{Re}[f_{CM}]$ is the real part of the Clausius-Mossotti (CM) factor which is:

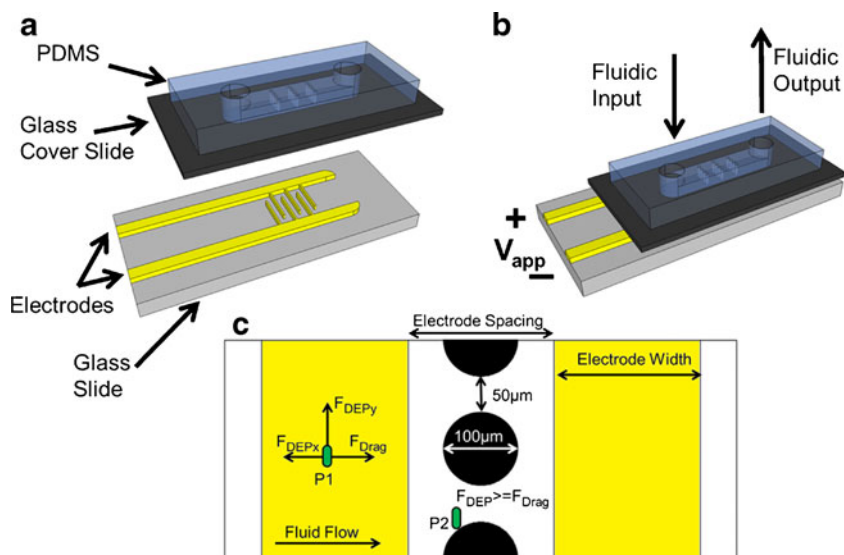
$$f_{CM} = (\epsilon_p^* - \epsilon_m^*) / (\epsilon_p^* + 2 \epsilon_m^*) \tag{2}$$

where ϵ_p^* and ϵ_m^* are the complex permittivities of the particle and the medium, respectively. Complex permittivity is defined as:

$$\epsilon^* = \epsilon + \sigma / (j\omega) \tag{3}$$

Thus, F_{DEP} will fluctuate greatly depending on the operating frequency and even change direction. At DC and very

Fig. 1 Schematic of the OπDEP device. (a) Isometric view of the device with the disposable fluidic section separated from the reusable electrodes; (b) device under operating conditions with the two parts assembled; (c) close-up view of the functional region of the device showing the relevant forces and dimensions. During operation, the microposts within the channel are aligned with the electrodes as shown



low frequency fields, DEP separation of bioparticles is mostly dominated by the size difference of the particles due to the cubed radius term and the low conductivity of cellular membranes. However, at high frequencies, the fields are able to penetrate the cell membrane into the electrically conductive cytoplasm. Consequently, cells can have a higher DEP frequency dependency than solid particles. If a particle is attracted to a region with a high electric field, it experiences positive DEP (pDEP). Conversely, if a particle is repelled by a region with a high electric field, it experiences negative DEP (nDEP). As the DEP force on a particle passes from pDEP to nDEP or vice versa in frequency space, a frequency point exists where the DEP force on a particle is zero, regardless of the magnitude of the electric field gradients. This point is known as a crossover frequency.

Fluid is moved through the channel by a pressure-driven flow. The drag force on a spherical particle in a fluid at a low Reynold's number is given by:

$$F_{\text{Drag}} = 6\eta R\pi(u_{\text{pf}}) \quad (4)$$

Where R is the radius of the particle, η is the viscosity of the fluid, and u_{pf} is the relative velocity of the particle with respect to the fluid. For a particle in our DEP devices, a force balance occurs between drag and dielectrophoresis as shown by particle P1 in Fig. 1c. In order for a particle to become trapped in these devices, the DEP force must overcome the drag force on the particle ($F_{\text{DEP}} \geq F_{\text{Drag}}$) as shown by particle P2 in Fig. 1d. Thus, DEP trapping becomes more difficult as the fluid velocity is increased.

As Eq. 1 shows, the DEP force is proportional to the gradient of the electric field squared. In our design, insulating structures within the channel enhance this gradient and greatly increase the DEP force over the interdigitated electrode design. This enables the device to operate at high flow rates and low frequencies.

Methods

Device designs

Three different designs are used in this work (Table 1). The microfluidic channel for all the devices has a cross section of

Table 1 Design parameters for each of the different devices

	Electrode width	Electrode spacing	Microposts present?
Device 1	200 μm	200 μm	No
Device 2	200 μm	200 μm	Yes
Device 3	4 mm	600 μm	Yes

2 mm \times 50 μm and a length of 2 cm. Device 1 is similar to a previously reported design [17] consisting of a microfluidic channel with no features and electrodes with a width of 200 μm and a spacing of 200 μm . This design is present in this work to compare with the innovative designs. The DEP forces in this device rely on nonuniform fields created by the presence of the off-chip electrodes. Devices 2 and 3, which are the new designs and the focus of this study, use a microfluidic channel with 100 μm diameter PDMS posts that are spaced 50 μm apart. In these devices, the insulating structures create the nonuniform fields necessary for DEP. Device 2 uses electrodes with a width of 200 μm and a spacing of 200 μm , the same as Device 1, for evaluation purposes. Device 3 has much larger electrodes with a width of 4 mm and a spacing of 600 μm . The wider electrodes of Device 3 increase the capacitive coupling between the electrodes and the microfluidic channel, which enables DEP trapping at lower frequencies.

Analytical and numerical device modeling

In order to investigate the electric field distributions within the microchannel, a numerical model of the devices was created using COMSOL Multiphysics 3.5 (COMSOL Inc., Burlington, MA, USA) using the AC/DC module. Three-dimensional models were created of the three devices in this study. The electrical conductivities used for PDMS, glass, air, and deionized water are 8.20e-13 S/m, 1.25e-9 S/m, 3.00e-9 S/m, and 8.00e-4 S/m, respectively. The electrical permittivities used for PDMS, glass, air, and deionized water are 2.65, 4.65, 1, and 80, respectively. As for the boundary conditions, the electrodes were given AC electric potentials, and all other boundaries were set to electrical insulation. The purpose of the simulations was to evaluate the values of $\nabla|E|^2$ as a function of position and frequency. Equation 1 shows that for a given particle and medium, $\nabla|E|^2$ is proportional to the DEP force felt by a particle. Thus, the performance of the device should be predicted by these simulations.

Device fabrication

The two-port microchannel devices are 2-cm long, 2-mm wide, and 50- μm deep fabricated in polydimethylsiloxane (PDMS). A <100> silicon wafer was patterned with photoresist (AZ9200) and etched using an Alcatel AMS-100 Deep Reactive Ion Etcher (Alcatel, Annecy, France) (DRIE) to obtain the structures. Photoresist was stripped and the wafer was then used as a master mold for PMDS. Liquid PDMS (Sylgard 184 Silicon elastomer kit; Dow Corning, Midland, MI, USA) was mixed to a 10:1 ratio of PDMS monomer and curing agent and poured onto the silicon mold. The setup was put into a vacuum chamber for 2 h to remove gas bubbles and then cured for 45 min at 100 $^{\circ}\text{C}$. Next, 2 mm holes were

punched into microchannels for fluidic ports. Finally, the PDMS was plasma bonded to a #0 micro cover glass (Electron Microscopy Sciences, Hatfield PA, USA) which is approximately 100 μm thick, forming the microfluidic cartridge.

On a separate Pyrex substrate, electrodes were formed using the lift-off technique. The substrate was patterned with photoresist (AZ9260; AZ Electronic Materials, London, UK). Next, using e-beam evaporation (PVD-250; Kurt J. Lesker Company, Jefferson Hills, PA, USA), a thin layer (25 nm) of chrome and then a thicker layer (200 nm) of gold was deposited. The excess metal was removed by dissolving the photoresist in acetone. As a technical note, a printed circuit board could be used for the electrode patterning if the transparency of the substrate is not crucial.

During device operation the microfluidic cartridge is placed onto the electrode substrate and aligned such that the insulating structures in the microchannel are visible between the electrodes. It should be noted that the alignment does not have to be very precise. As long as the microposts are present between in the electrodes, the devices will operate. The electric fields are capacitively coupled into the microfluidic channel and the nonuniform fields necessary for DEP are created by the insulating structures in the channel. After running an experiment, the PDMS microfluidic device was easily removed from the electrodes and a new device was placed on the electrodes.

Cell preparation

E. coli strain MG1655 was grown at 37 °C in LB medium containing 1 % tryptone, 0.5 % NaCl, and 0.5 % yeast to a concentration of 4×10^8 cells/mL. Tetracycline was applied as the antibiotic at 5 $\mu\text{g}/\text{mL}$ concentration since the strain contained pHC60, a stably maintained plasmid that constitutively expresses green fluorescent protein (GFP) useful for fluorescent microscopy analyses. For all experiments, *E. coli* cells, red fluorescent 1 μm beads (Fluorospheres; Invitrogen, Carlsbad, CA, USA), or both were centrifuged and resuspended three times in DI water with a measured conductivity of 800 $\mu\text{S}/\text{m}$. No surface modifications were made to the beads. The DI water conductivity was measured with a solution conductivity meter (SG7; Mettler Toledo, Scherzenbach, Switzerland). The cells were diluted to a final concentration of 1×10^8 cells/mL. For experiments with a mixture of fluorescent beads and *E. coli*, the fluorescent beads were diluted to a concentration of 1×10^8 beads/mL. It should be noted that due to a lack of nutrients in the DI water, the *E. coli* cells will eventually die if they are not resuspended in a medium with nutrients. However, using a fluorescent stain viability kit (Live/Dead BacLight; Invitrogen), the *E. coli* cells were found to be over 95 % viable after being suspended in the DI water for 1 h. This ensured that the experiments were being performed on live *E. coli* cells.

Experimental setup

A function generator (4079; BK Precision, Yorba Linda, CA, USA) was connected to a power amplifier (EW2350; Tegam, Geneva, OH, USA) which excited the reusable electrodes with an AC signal of 400 V peak to peak (V_{p-p}) with frequencies from 1 kHz to 1 MHz. An oscilloscope (DL1300A; Yokogawa, Tokyo, Japan) was connected to the monitor output of the amplifier to observe the applied waveforms for distortion. The PDMS-based microfluidic devices were placed in vacuum for at least 30 min before experiments were run to reduce priming issues. During device operation, the solution was passed through the $O\pi$ DEP device using a 1 mL syringe connected to syringe pump (NE-1000; New Era Pumping Systems, Farmingdale, NY, USA) to a waste reservoir. Once the device was primed, fluid was continually moved through the channels at 50 $\mu\text{L}/\text{h}$ for 5 min prior to the beginning of the experiments. DEP trapping experiments were observed using an inverted fluorescent microscope (Axio Observer Z1) and videos of all trapping experiments were acquired using either a CCD monochrome camera (AxioCam MRm) or a CCD color camera (AxioCam MRc). For experiments where red beads and green stained *E. coli* were mixed, the optical filter was changed between red and green from frame to frame to distinguish the different particles.

For a single DEP trapping experiment data point, the flow rate of interest would be applied for 15 s to stabilize the flow velocity. Then, the electric signal would be switched on and the DEP trapping would be recorded by video. The signal switched off after 30 s and bacteria were released. The microchannels were inspected before every run and cleared of fouled bacteria by increasing the flow rate of the syringe pump when necessary. Thus, each data point included only bacteria trapped during that run.

One method of quantifying the effectiveness of the DEP trap is the use of light intensity measurements. The *E. coli* cells used in this work expressed GFP, which acted as a fluorescent stain. During DEP trapping experiments, as the number of *E. coli* cells trapped in the $O\pi$ DEP device increased, the intensity of the light also increased. Using ImageJ (NIH), a region of interest was chosen around the microposts, where the DEP trapping occurred, and the intensity of the light in this region was quantized for the last frame before the electric signal was removed. The size, shape, and location of the region of interest were held constant throughout the experiments. These experiments were repeated 10 times in random order and the results were averaged at each applied signal frequency.

Another performance metric for the experiments is the capture efficiency (CE), which is defined as:

$$\text{CE} = [(I-O)/I] \times 100\% \quad (5)$$

where I is the number of incoming bacteria observed on a single frame of the trapping video, O is the number of

outgoing or escaped bacteria observed on a single frame of the trapping video. These measurements were made by counting the bacteria upstream (I) and downstream (O) of the trapping region in the individual frames of the videos taken during the experiments. The regions used for counting I and O were the identically sized rectangles and remained constant for the experiments. Ten fluid flow velocity sweeps from 100 $\mu\text{L/h}$ to 1500 $\mu\text{L/h}$ were each completed in random order. To obtain a data point representing one flow rate, values of I and O were averaged over the 10 flow sweeps. For cases where bacteria remained in clusters after being released, the clusters were assumed to be flat and the size of the cluster was used to estimate the number of bacteria in the cluster. It should be noted that if clusters had multiple bacteria stacked in depth, this method would underestimate the number of bacteria.

Results and discussion

Numerical modeling

The results from the numerical model are displayed in Fig. 2. In Fig. 2a and b, the 3D geometry used is shown next to the $\nabla(\mathbf{E}\cdot\mathbf{E})$ slice plot for an applied signal of 400 V_{p-p} at 300 kHz. It should be noted that the simulation for Device 3 is not shown here as it is much larger than Devices 1 and 2 because of the 4-mm electrodes. However, the electric field distribution for Device 3 is virtually identical to that of Device 2. Figure 2a shows the electric field gradients in Device 1 with a peak gradient of about 3.2×10^{13} $[(\text{m}\cdot\text{kg}^2)/(\text{s}^6\cdot\text{A}^2)]$. Figure 2b shows the electric field gradient in Device 2 with a peak gradient of about 2.3×10^{15} $[(\text{m}\cdot\text{kg}^2)/(\text{s}^6\cdot\text{A}^2)]$. This means for a given applied signal,

the introduction of the insulating posts within the channel increases values of $\nabla(\mathbf{E}\cdot\mathbf{E})$ by two orders of magnitude compared with the previously reported electrode-only design. This is an important result as Eq. 1 shows that $\nabla(\mathbf{E}\cdot\mathbf{E})$ is proportional to the DEP force on a particle. The other significant result is the location of the high field gradients. For Device 1, the highest field gradients occur directly over the electrodes, whereas for Device 2 the highest field gradients occur near the insulating structures and away from the electrodes. This is a common characteristic of iDEP devices [14]. The advantage of having the peak electric field gradients away from the electrodes is a practical one. Particle fouling in the microchannel tends to occur in DEP devices where the strongest DEP forces are present. For eDEP devices, such as Device 1, this is at the electrodes. This can effectively add another passivation layer to the electrodes, which will weaken the electric fields and lower the performance of the device. However, for iDEP devices, such as Device 2, fouling will tend to occur at the insulating structures and not over the electrodes. Thus, the electric fields will remain high in the device until enough particles have fouled to completely clog the device.

Figure 2c shows the frequency response of the DEP devices. As the plot shows, $O\pi$ DEP devices create much larger electric fields over a large frequency range. Furthermore, Device 3 creates larger electric field gradients at low frequencies compared with Device 2. This is due to the increased capacitance of the very large electrodes for Device 3. The maximum gradient reached with Device 3 is less than that of Device 2; however, this is due to the increased electrode spacing. The larger spacing was simply a practical consideration as it made alignment simpler. This increased capacitance effectively shifts the graph of the frequency response to lower frequencies. Thus, the local minimum

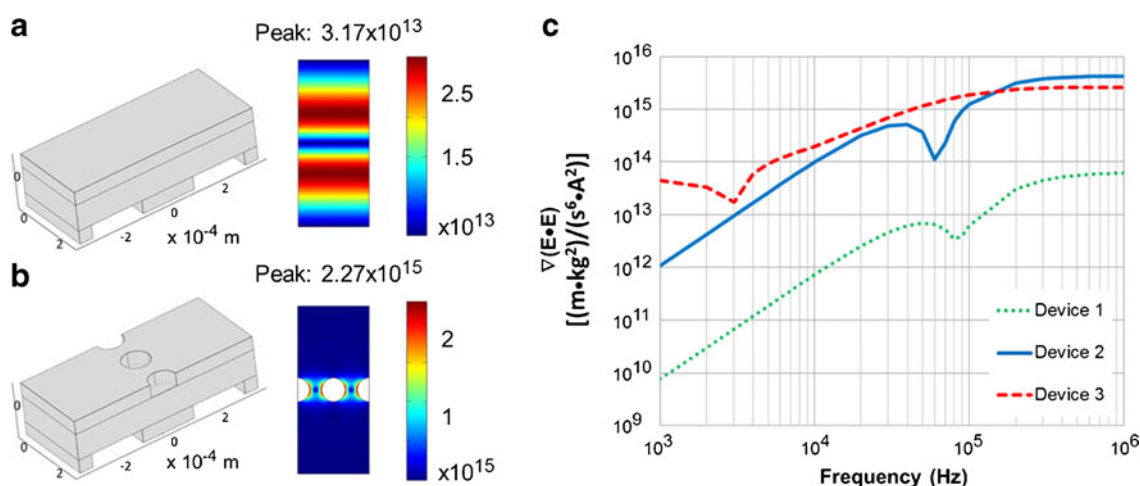


Fig. 2 COMSOL simulations of electric field gradients in the $O\pi$ DEP devices. The PDMS roof of the devices has been removed from the figure for clarity; (a) $\nabla(\mathbf{E}\cdot\mathbf{E})$ at 300 kHz in previously reported Device 1

without microfluidic structures; (b) $\nabla(\mathbf{E}\cdot\mathbf{E})$ at 300 kHz in $O\pi$ DEP Device 2; (c) maximum values of $\nabla(\mathbf{E}\cdot\mathbf{E})$ as a function of frequency

between 10^4 Hz and 10^5 Hz on for Device 2 is moved to between 10^3 Hz and 10^4 Hz. In summary, electrode design in Device 3 yields higher electric field gradients over a wider frequency range but at the cost of a larger device size and less compactness.

Frequency response

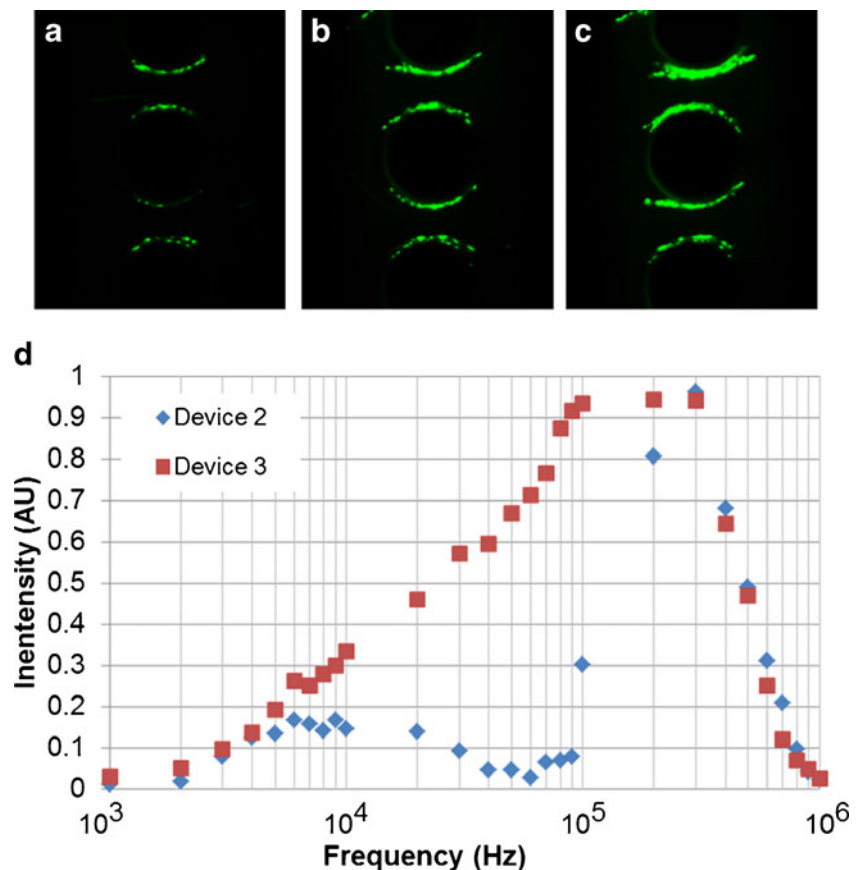
Bacteria trapping experiments were performed on all devices with the applied electric signal of $400 V_{p-p}$. When there was no fluid flow in the channel, bacteria in Device 1 were observed moving toward the electrodes and forming pearl chains. This is typical behavior in DEP devices operating in the pDEP regime [18–20]. However, when any fluid flow was introduced, the DEP forces inside Device 1 were not strong enough to overcome the drag force on the bacteria. Therefore, no trapping was observed in Device 1 even at the lowest applied flow rate of $10 \mu\text{L/h}$. Conversely, in Devices 2 and 3 not only did bacteria trap with applied fluid flow, the trapping attained 100 % capture efficiency with flow rates up to $400 \mu\text{L/hr}$. This clearly demonstrates that the $O\tau\text{DEP}$ devices greatly outperform the off-chip electrode based devices [17] in DEP trapping strength.

Figure 3 shows the experimental performance of the $O\tau\text{DEP}$ devices at different applied frequencies but with a fixed flow rate of $400 \mu\text{L/h}$. As Figure 3a–c show, the ability

of the devices to trap *E. coli* cells varied with frequency. Figure 3d shows the quantification of the light intensity in the trapping region for Devices 2 and 3 as a function of frequency. Device 1 is excluded from Fig. 3d as DEP trapping could not be attained with applied fluid flow. It should be noted that the amplitude of the amplified signal began to attenuate at 400 kHz due to the power amplifier limitation. This led to a decrease in DEP trapping strength at higher frequencies. For Device 2, maximum trapping occurred at 300 kHz. At this frequency, no bacteria were observed escaping the trap and thus the CE was 100 %. Device 3 attained a CE of 100 % at a lower frequency, 100 kHz, and maintained 100 % trapping until the bandwidth limit of the amplifier was reached.

These results match well with the numerical models. In the numerical models, the highest DEP forces are shown to be close to the microposts and decrease as the distance from the posts is increased. Thus, the minimum DEP force that a particle passing through the channel will experience is along the centerline between two posts. For weak DEP forces, particles near the posts may trap but not the particles traveling along the centerline. As the magnitude of the DEP force is increased, more particles will trap, increasing the efficiency of the device. When the magnitude of the DEP force is strong enough to trap a particle along the centerline, 100 % CE will be obtained. Thus, increases in the DEP forces will

Fig. 3 Observed DEP trapping of *E. coli* in the $O\tau\text{DEP}$ devices for an applied AC signal at $400V_{p-p}$ and a flow rate of $400 \mu\text{L/h}$. Trapping images are shown for Device 2; (a) 10 kHz signal; (b) 100 kHz signal; (c) 300 kHz signal; (d) quantized light intensity in the trapping region as a function of frequency ($n=10$)



result in higher trapping efficiencies. Since the electric field gradients in the device are dependent on frequencies, the trapping efficiencies will be as well.

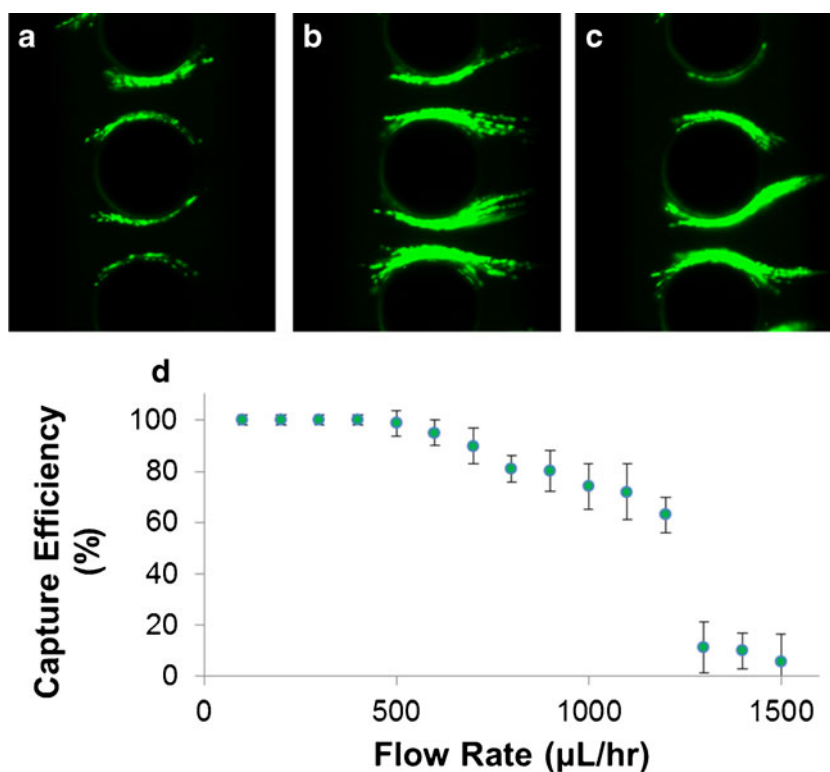
The DEP force on a particle is dependent not only on the electric field gradients but also on the properties of the particle and the suspending medium. For *E. coli* suspended in a media with a conductivity of ~ 1 mS/m, the CM factor has been shown to increase monotonically from DC until after 1 MHz [21] leading to a monotonic increase in DEP trapping until 1 MHz [22]. Considering the particles and medium are held constant, the differences in performance of the devices are solely based on the differences in the electric field gradients ($\nabla(\mathbf{E}\cdot\mathbf{E})$) generated in the channel.

The local minimum in $\nabla(\mathbf{E}\cdot\mathbf{E})$ in Device 2 between 10^4 and 10^5 Hz predicted by the model appears in the experimental data as decreased trapping from 10^4 to 10^5 Hz. However, in Device 3, the local minimum is predicted to be between 10^3 and 10^4 Hz, where the DEP trapping is already weak. Thus, in the experiments, Device 3 did not have decreased trapping from 10^4 to 10^5 as Device 2 did. Instead, the *E. coli* trapping increased monotonically with frequency. It should be noted that some of the increased performance of Device 3 may be due to the fact that the wide electrodes may mitigate any losses from air gaps created by slightly warped glass cover slides. The thin electrodes of Device 2, however, would not be as resilient to imperfections in the assembly.

Flow rate tests

To determine the throughput of the devices, the flow rate was swept from 100 $\mu\text{L/h}$ to 1500 $\mu\text{L/h}$. The applied electric signal was held constant at 400V_{p-p} and 300 kHz as this was the frequency at which both Device 2 and Device 3 experienced the highest trapping efficiency. Figure 4 shows the dependence of capture efficiency on flow rate. It should be noted that both devices performed very similarly with the mean values with 4 % of each other, making the data points between the two difficult to distinguish. Thus, for clarity, Fig. 4d shows only the data from Device 2. The devices were able to obtain 100 % CE consistently for flow rates up to 400 $\mu\text{L/h}$. A decrease in capture efficiency began at 500 $\mu\text{L/h}$, where a few of the runs had a CE of 100 % but it was not consistent. From 500 $\mu\text{L/h}$ to 1200 $\mu\text{L/h}$, the capture efficiency decreased gradually in a roughly linear fashion. However, at 1300 $\mu\text{L/h}$, the CE plummeted. In the videos of the experiments, DEP trapping was still observed. However, as pearl chains of *E. coli* formed, eventually the drag force on the pearl chain would become strong enough to pull the entire group of bacteria off of the microposts. This would repeat itself throughout the experiments, leading to very little net trapping. These results show that the maximum throughput for 100 % trapping is 400 $\mu\text{L/h}$. If only concentration is desired and capture efficiency is not critical, the devices can be operated at flow rates up to 1200 $\mu\text{L/h}$.

Fig. 4 Observed DEP trapping of *E. coli* in the $O\pi$ DEP devices for an applied AC signal at 400V_{p-p} at 300 kHz and variable flow rates. Trapping images are shown for Device 3; (a) 500 $\mu\text{L/h}$; (b) 900 $\mu\text{L/h}$; (c) 1200 $\mu\text{L/h}$; (d) capture efficiency as a function of flow rate ($n=10$ sweeps). Error bars shown for one SD



Selective concentration

To demonstrate the ability of these devices to selectively concentrate biological samples from contaminants, *E. coli* cells were mixed with 1 μm red fluorescent beads, which were chosen because they are roughly the same size as *E. coli* cells. As Fig. 5 shows, the bacteria were trapped and released on the microposts, whereas the beads did not (see Electronic Supplementary Material Video S1). It should be noted that some of the red beads did foul to the surfaces of the device before any electric signal was applied, as Fig. 5a shows. However, only the bacteria were reversibly trapped with dielectrophoresis. This is evident when observing frames immediately after turning the electric signal off. As Fig. 5c shows, only bacteria are present in the released sample. The bacteria are, therefore, completely separated from the beads, demonstrating the potential of $O\pi\text{DEP}$ for selectively concentrating samples.

Conclusion

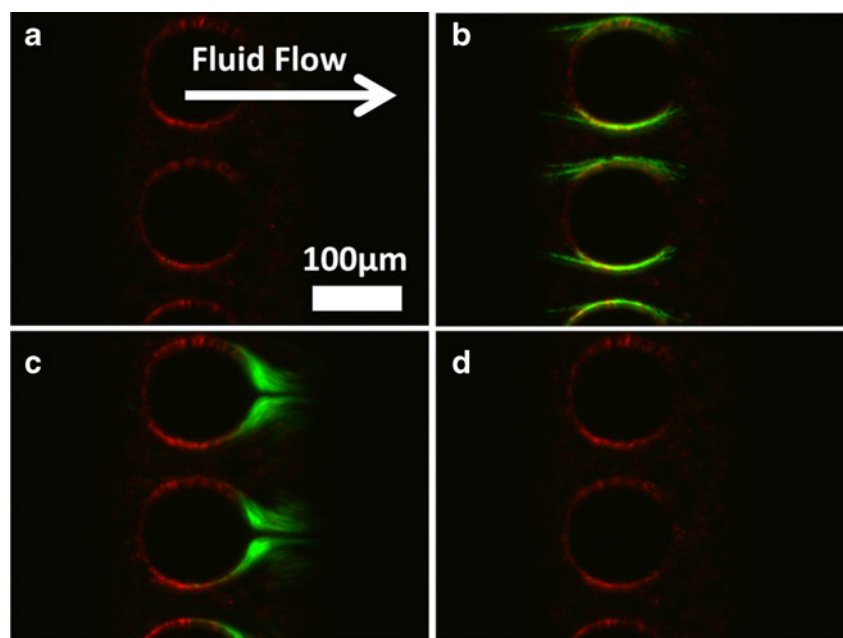
$O\pi\text{DEP}$ is a recently invented method by our group to actuate iDEP devices with reusable electrodes on a separate substrate, allowing for a very scalable throughput. The $O\pi\text{DEP}$ technique allows for inexpensive polymer microfluidic cartridges to be disposable while having reusable electrodes. In this paper, we have (1) presented $O\pi\text{DEP}$, the first reported iDEP devices powered by off-chip electrodes, (2) demonstrated through modeling and experiments the superior performance of $O\pi\text{DEP}$ devices over the electrode-only designs, (3) demonstrated how different electrode patterns can be used to affect the trapping performance,

and (4) demonstrated selective *E. coli* manipulation with the $O\pi\text{DEP}$ devices.

This technique combines the advantages of traditional eDEP (tunable electrodes and strong electric fields) with those of iDEP (tunable insulating structures, no electrode fouling, and inexpensive devices). While the applied signal parameters such as the AC voltage magnitude and AC signal frequency can be tuned in real time, the physical parameters, such as electrode spacing, electrode shape, and geometrical dimensions can also be adjusted to fit the application. It is particularly important to note that because of the ability of this technology to reuse the electrodes, a toolkit of reusable electrodes can be created to suit a large range of applications. As shown in this work, the electrodes can be made very wide for better low frequency operation or very narrow for a compact footprint. Groups of electrodes can be put in parallel for high throughput batch processing. Alternatively, unlike traditional iDEP devices, $O\pi\text{DEP}$ devices can have many independent electrodes and give each set of electrodes a different electric signal. This would create a very compact platform with multiple trapping zones in series, each with unique geometrical features tailored for multi-step filtration/isolation or for enrichment of different biological particles in a single operation.

While $O\pi\text{DEP}$ relies on iDEP principles to generate trapping, it alleviates one of the main disadvantages of iDEP, which is Joule heating. iDEP devices typically have electrodes that actuate the devices at the fluid inlet and outlet. Thus, resistive heating occurs along the entire length of the channel. This heat buildup can limit the throughput of iDEP device and even result in device failure [15]. Additionally, for biological

Fig. 5 Selective trapping of *E. coli* (green) from 1 μm beads (red) with a fluid flow rate of 400 $\mu\text{L}/\text{h}$. (a) No applied voltage; (b) 400 V_{p-p} at 300 kHz is applied for 30 s; (c) voltage is turned off and the concentrated bacteria is released; (d) after trapped bacteria are released, none remains on the microposts



applications, higher temperatures can affect the sample or even reduce viability rates [23]. The $O\pi$ DEP devices, however, greatly reduce the electrode spacing, creating electric field gradients in a very small area of the microchannel. This reduces the total electrical energy converted to heat and, thus, Joule heating is minimized. The result is that $O\pi$ DEP compared with iDEP devices may be able to operate for longer times, with a wider range of media, and with minimized temperature effects on the biological samples.

Another advantage of $O\pi$ DEP design is the throughput. As we have demonstrated, high capture efficiencies are achievable at high flow rates because of the strong DEP forces generated in $O\pi$ DEP devices. It also should be noted that since the electrodes generating the field are implemented across the channel width, the channel can be made arbitrarily wide and the DEP forces will remain the same. Thus, the throughput can be increased by simply widening the microchannel. There may, however, be some practical limitations to the fabrication of very wide channels without the channels collapsing. These problems will be mitigated by the microposts within the channel acting as support columns.

$O\pi$ DEP devices can be customized to meet a broad range of applications. Even though we have used microposts design, any iDEP microchannel configuration can be employed with this technology, including single constrictions [24], 3D constrictions [25–27], 3D barriers [28], and filter designs [29]. DEP deflection-based devices [12, 30–32], which operate continuously with lower DEP forces, are straightforward to implement with $O\pi$ DEP. Since deflection-based designs do not need to completely stop particles in the channels, they can be operated with lower applied voltages.

This technology has the potential to provide rapid, reproducible, and cost-effective platform of DEP particle manipulation for applications ranging from pathogen detection to cancer cell characterization. In our future work, we plan to explore devices with passivation membrane thicknesses much less than the 100 μm cover slides used in this paper. We anticipate that these devices will be able to trap at much lower applied voltages, work over a wider frequency range, and have increased throughputs. Additionally, we will explore DEP device designs with different micropost configurations to further increase the capture efficiencies at very high flow rates.

Acknowledgement This work was supported primarily by the National Science Foundation CAREER award (ECCS-0747600).

Open Access This article is distributed under the terms of the Creative Commons Attribution License which permits any use, distribution, and reproduction in any medium, provided the original author(s) and the source are credited.

References

- Zhou R, Wang P, Chang H-C (2006) Bacteria capture, concentration and detection by alternating current dielectrophoresis and self-assembly of dispersed single-wall carbon nanotubes. *Electrophoresis* 27(7):1376–1385
- Huang Y, Holzel R, Pethig R, Wang XB (2000) Differences in the AC electrodynamics of viable and non-viable yeast cells determined through combined dielectrophoresis and electrorotation studies. *Phys Med Biol* 37(7):1499
- Hunt T, Westervelt R (2006) Dielectrophoresis tweezers for single cell manipulation. *Biomed Microdevices* 8(3):227–230
- Grom F, Kentsch J, Müller T, Schnelle T, Stelzle M (2006) Accumulation and trapping of hepatitis A virus particles by electrohydrodynamic flow and dielectrophoresis. *Electrophoresis* 27(7):1386–1393
- Hölzel R, Calander N, Chiragwandi Z, Willander M, Bier FF (2005) Trapping single molecules by dielectrophoresis. *Phys Rev Lett* 95(12):128102
- Alazzam A, Stiharu I, Bhat R, Meguerditchian A-N (2011) Interdigitated comb-like electrodes for continuous separation of malignant cells from blood using dielectrophoresis. *Electrophoresis* 32(11):1327–1336
- Li HB, Bashir R (2002) Dielectrophoretic separation and manipulation of live and heat-treated cells of *Listeria* on microfabricated devices with interdigitated electrodes. *Sensors Actuators B* 86(2/3):215–221
- Wang L, Lu J, Marukenko SA, Monuki ES, Flanagan LA, Lee AP (2009) Dual frequency dielectrophoresis with interdigitated sidewall electrodes for microfluidic flow-through separation of beads and cells. *Electrophoresis* 30(5):782–791
- Hsiung LC, Yang CH, Chiu CL, Chen CL, Wang Y, Lee H, Cheng JY, Ho MC, Wo AM (2008) A planar interdigitated ring electrode array via dielectrophoresis for uniform patterning of cells. *Biosens Bioelectron* 24(4):869–875
- Lapizco-Encinas BH, Simmons BA, Cummings EB, Fintschenko Y (2004) Insulator-based dielectrophoresis for the selective concentration and separation of live bacteria in water. *Electrophoresis* 25(10/11):1695–1704
- Martinez-Lopez JI, Moncada-Hernandez H, Baylon-Cardiel JL, Martinez-Chapa SO, Rito-Palomares M, Lapizco-Encinas BH (2009) Characterization of electrokinetic mobility of microparticles in order to improve dielectrophoretic concentration. *Anal Bioanal Chem* 394(1):293–302
- Chen D, Du H (2010) A microfluidic device for rapid concentration of particles in continuous flow by DC dielectrophoresis. *Microfluid Nanofluid* 9(2/3):281–291
- Ozuna-Chacon S, Lapizco-Encinas BH, Rito-Palomares M, Martinez-Chapa SO, Reyes-Betanzo C (2008) Performance characterization of an insulator-based dielectrophoretic microdevice. *Electrophoresis* 29(15):3115–3122
- Davalos RV, McGraw GJ, Wallow TI, Morales AM, Krafcik KL, Fintschenko Y, Cummings EB, Simmons BA (2008) Performance impact of dynamic surface coatings on polymeric insulator-based dielectrophoretic particle separators. *Anal Bioanal Chem* 390(3):847–855
- Sabounchi P, Huber DE, Kanouff MP, Harris AE, Simmons BA (2008) Joule heating effects on insulator-based dielectrophoresis. Paper presented at the 12th International Conferences on Miniaturized Systems for Chemistry and Life Sciences, San Diego, CA, USA, Oct 12–16
- Pohl H (1951) The motion and precipitation of suspensions in divergent electric fields. *Appl Phys* 22:869–871
- Park K, Suk HJ, Akin D, Bashir R (2009) Dielectrophoresis-based cell manipulation using electrodes on a reusable printed circuit board. *Lab Chip* 9(15):2224–2229

18. Markx GH, Talary MS, Pethig R (1994) Separation of viable and non-viable yeast using dielectrophoresis. *J Biotechnol* 32(1):29–37
19. Shafiee H, Sano MB, Henslee EA, Caldwell JL, Davalos RV (2010) Selective isolation of live/dead cells using contactless dielectrophoresis (cDEP). *Lab Chip* 10(4):438–445
20. Li H, Bashir R (2002) Dielectrophoretic separation and manipulation of live and heat-treated cells of *Listeria* on microfabricated devices with interdigitated electrodes. *Sensors Actuators B Chem* 86(2/3):215–221
21. Castellarnau M, Errachid A, Madrid C, Juárez A, Samitier J (2006) Dielectrophoresis as a tool to characterize and differentiate isogenic mutants of *Escherichia coli*. *Biophys J* 91(10):3937–3945
22. Cho YK, Kim S, Lee K, Park C, Lee JG, Ko C (2009) Bacteria concentration using a membrane type insulator-based dielectrophoresis in a plastic chip. *Electrophoresis* 30(18):3153–3159
23. Voldman J (2006) Electrical forces for microscale cell manipulation. *Annu Rev Biomed Eng* 8:425–454
24. Staton SJR, Chen KP, Taylor TJ, Pacheco JR, Hayes MA (2010) Characterization of particle capture in a sawtooth patterned insulating electrokinetic microfluidic device. *Electrophoresis* 31(22):3634–3641
25. Zellner P, Agah M (2012) Silicon insulator-based dielectrophoresis devices for minimized heating effects. *Electrophoresis* 33(16):2498–2507
26. Hosseini Y, Zellner P, Agah M (2012) A single-mask process for 3D microstructure fabrication in PDMS. *J Microelectromech Syst* 22(2):356–361
27. Braff WA, Pignier A, Buie CR (2012) High sensitivity three-dimensional insulator-based dielectrophoresis. *Lab Chip* 12(7):1327–1331
28. Hawkins BG, Smith AE, Syed YA, Kirby BJ (2007) Continuous-flow particle separation by 3D insulative dielectrophoresis using coherently shaped, dc-biased, ac electric fields. *Anal Chem* 79(19):7291–7300
29. Suehiro J, Zhou G, Imamura M, Hara M (2003) Dielectrophoretic filter for separation and recovery of biological cells in water. *IEEE Trans Ind Appl* 39(5):1514–1521
30. Demierre N, Braschler T, Linderholm P, Seger U, van Lintel H, Renaud P (2007) Characterization and optimization of liquid electrodes for lateral dielectrophoresis. *Lab Chip* 7(3):355–365
31. Zhu J, Xuan X (2011) Curvature-induced dielectrophoresis for continuous separation of particles by charge in spiral microchannels. *Biomicrofluidics* 5(2):24111. doi:10.1063/1.3599883
32. Sano MB, Caldwell JL, Davalos RV (2011) Modeling and development of a low frequency contactless dielectrophoresis (cDEP) platform to sort cancer cells from dilute whole blood samples. *Biosens Bioelectron* 30(1):13–20